Visualization of *trp* Repressor and its Complexes with DNA by Atomic Force Microscopy

Emmanuel Margeat, Christian Le Grimellec, and Catherine A. Royer
Centre de Biochimie Structurale, INSERM U 414-CNRS UMR 9955-Université Montpellier I, Montpellier, France

ABSTRACT We used tapping mode atomic force microscopy to visualize the protein/protein and the protein/DNA complexes involved in transcriptional regulation by the *trp* repressor (TR). Plasmid fragments bearing the natural operators *trp* EDCBA and *trp* R, as well as nonspecific fragments, were deposited onto mica in the presence of varying concentrations of TR and imaged. In the presence of L-tryptophan, both specific and nonspecific complexes of TR with DNA are apparent, as well as free TR assemblies directly deposited onto the mica surface. We observed the expected decrease in specificity of TR for its operators with increasing protein concentration (1–5 nM). This loss of DNA-binding specificity is accompanied by the formation of large protein assemblies of varying sizes on the mica surface, consistent with the known tendency of the repressor to oligomerize in solution. When the co-repressor is omitted, no repressor molecules are seen, either on the plasmid fragments or free on the mica surface, probably because of the formation of larger aggregates that are removed from the surface upon washing. All these findings support a role for protein/protein interactions as an additional mechanism of transcriptional regulation by the *trp* repressor.

INTRODUCTION

The *trp* repressor (TR) of *Escherichia coli* provides the primary control element for the synthesis of tryptophan in this organism. L-Tryptophan at relatively high concentrations ($\sim\mu$M) binds to TR, leading to a structural and dynamic change in the protein that increases its affinity for specific operator sites in the *E. coli* genome, situated upstream of operons whose gene products are responsible for the synthesis of tryptophan and other aromatic amino acids (*trp* EDCBA, *aro*H, *mtr*) (Rose and Yanofsky, 1974; Zurawski et al., 1981; Heatwole and Sommerville, 1991). TR also binds to an operon upstream of the gene encoding its own synthesis (*trp* R) and thus also functions as an autorepressor (Gunsalus and Yanofsky, 1980). Binding of TR to its target sites presumably competes with RNA polymerase binding to its promoter sequence and effectively represses gene expression.

Examination of TR binding sites, both natural and artificial, and the affinity and stoichiometry of TR interactions at these sites (Kumamoto et al., 1987; Staake et al., 1990; Haran et al., 1992; Liu and Matthews, 1993; Czernik et al., 1994; Yang et al., 1996; Bareket-Samish et al., 1997; Reedstrom et al., 1997; Haran, 1998) has revealed the internal twofold symmetry of TR half-sites and the higher-order protein/protein interactions involved in specific complex formation. A crystal structure of tandemly bound TR dimers shows that the recognition helices of the helix-turn-helix DNA binding domain of adjacent dimers share the central major groove in the CTAG half-site sequence (Bennett and Yanofsky, 1978) and that tyrosine 7 plays a role in stabilizing the contacts between dimers (Lawson and Carey, 1993). In addition to higher-order TR complexes at its operator site, fluorescence, sedimentation, chromatographic, and cross-linking studies have revealed L-tryptophan-dependent interactions between TR dimers in solution in the absence of DNA (Fernando and Royer, 1992; Martin et al., 1994; Reedstrom and Royer, 1995; Reedstrom et al., 1996). Based on the L-tryptophan dependence of the interactions and the known autogenous regulation of TR, we proposed an additional control mechanism involving higher-order repressor oligomers competing with site-specific DNA binding.

Atomic force microscopy (AFM) has evolved in recent years into a relatively straightforward methodology for visualizing individual biomolecules and biomolecular complexes with a resolution near 10–100 nm (Hansma and Hoh, 1994; Yang and Shao, 1995; Bustamante et al., 1997; Hansma et al., 1997). In particular, interesting and revealing images of DNA (Yang et al., 1992, 1995; Schaper et al., 1994; Mou et al., 1995; Hansma et al., 1995; Cherny et al., 1998) and protein/DNA complexes (Erie et al., 1994; Le Cam et al., 1994; Guthold et al., 1994; Fritzsche et al., 1994, 1997; Lyubchenko et al., 1995, 1997; Wyman et al., 1995, 1997; Rippe et al., 1997; Kasas et al., 1997; Palecek et al., 1997) have been obtained in which DNA conformation and complex stoichiometry have been observed. Given the complexity of TR interactions both free and bound to specific or nonspecific DNA, AFM presents itself as a useful methodology for a structural characterization of the multiple interaction modes of this protein. We have therefore obtained images of TR both bound to DNA and in the free form by deposition on mica surfaces and tapping mode imaging in air.

Received for publication 18 May 1998 and in final form 10 September 1998.

Address reprint requests to Dr. Catherine A. Royer, Centre de Biochimie Structurale, INSERM U 414-CNRS UMR 9955-Université Montpellier I, Institut Universitaire de Recherche Clinique, 75, rue de la Cardonille 34093, Montpellier Cedex 5, France. Tel.: (33) 4 67 41 59 13; Fax: (33) 4 67 41 59 12; E-mail: royer@tome.cbs.univ-montp1.fr.

0006-3495/98/12/2712/09 $2.00

MATERIALS AND METHODS

Repressor purification

Repressor protein was overexpressed and purified by the method of Paluh and Yanofsky (Paluh and Yanofsky, 1986) as described by Fernando and Royer (1992) from *E. coli* strain CY15071 carrying overexpression plasmids pJPR-2 and pMS421. The concentration of aporepressor was determined using an extinction coefficient of 30,000 $M^{-1} \cdot cm^{-1}$ at 280 nm (Joachimiak et al., 1983).

Plasmids

The plasmids containing the operator sites for the *trp* repressor were a kind gift from Barry Hurlburt (Department of Biochemistry and Molecular Biology, University of Arkansas-Medical Sciences). The operators (*trp* EDCBA or *trp* R) were cloned as blunt 43-bp double-stranded DNA into the *Sma*I site of the polylinker of pUC118 (at 910 bp of the parental plasmid); *Dde*I-cut of these plasmids leads to six fragments of 1429, 540, 426, 409, 235, and 166 bp. Assuming a 0.34 nm/bp length for B-DNA, these fragments are expected to be respectively 485, 185, 145, 140, 80, and 55 nm long. The 426- and 409-bp fragments cannot be distinguished, either using agarose gel electrophoresis or on the AFM images.

The operator sites are located close to the center of the 485-nm-long fragment. This position is easy to locate on the AFM images, allowing us to identify specific protein/DNA complexes. We used unpurified plasmids cuts, instead of a preparation containing only the 1429-bp fragment, in order to use the other fragments as controls for nonspecific protein/DNA interactions.

Sample preparation

Protein/DNA binding reactions were conducted in 10 mM Tris buffer (pH 7.5) containing 10 mM $MgCl_2$ and 50 mM NaCl. Except when specified, 1 mM L-Trp was also present in solution. DNA concentration was 100 pM and repressor concentration was varied from 1 to 100 nM.

Five μl of solution were deposited for 1 min onto freshly cleaved ruby mica pieces (Goodfellow, Cambridge, UK). The sample was then rinsed with 3 × 2 ml of ultra-pure water and 2 ml of 0.1% uranyl acetate (Delain et al., 1992; Cherny et al., 1998). Excess liquid was blotted off with Whatman filter paper. The mica was then air dried for at least 30 min before imaging. The samples were stable for several days.

Scanning force microscopy

Samples were imaged with a Nanoscope III microscope, equipped with a type E scanner (Digital Instruments, Santa Barbara, CA), operating in tapping mode. All images were obtained in air at 21°C using 125-μm-long silicon nitride cantilevers (TESP type, Digital Instruments). The 512 × 512 pixel images were collected at a scan rate of two scan lines per second.

Description of AFM images

In tapping mode AFM, the oscillating cantilever is driven near its resonance frequency by a piezoelectric transducer that provides a driving force of constant amplitude. The tip at the end of the cantilever briefly touches the surface during each oscillation as it scans the sample. When this intermittent interaction occurs, it lowers the vibrational amplitude. To maintain the contact voltage at a specified set point, a feedback loop adjusts the height of the sample using a piezoelectric crystal. This motion provides the classical "height" signal. Using this operating mode, the tip-sample lateral force is greatly reduced and the short tip-sample contact time prevents excessive inelastic surface modification. This makes this method suitable for studying soft samples, such as biomolecules.

The phase signal measures the phase lag of the cantilever oscillation relative to the piezo drive. The decrease in amplitude arising directly from the tip-sample interactions and the phase variations generate two other signals representing the dynamic motion of the cantilever. This information arises from complex elastic and inelastic tip-sample interactions, so they can be used to study the dynamic behavior and properties of the sample (Tamayo and Garcia, 1997).

RESULTS AND DISCUSSION

Validation of DNA deposition protocol

Fig. 1 shows two representations of DNA deposited onto mica, as typically observed using our deposition protocol. The background is exempt of contamination, and the five different plasmid cuts can be recognized on these images. The measured lengths for these fragments were 497 ± 20

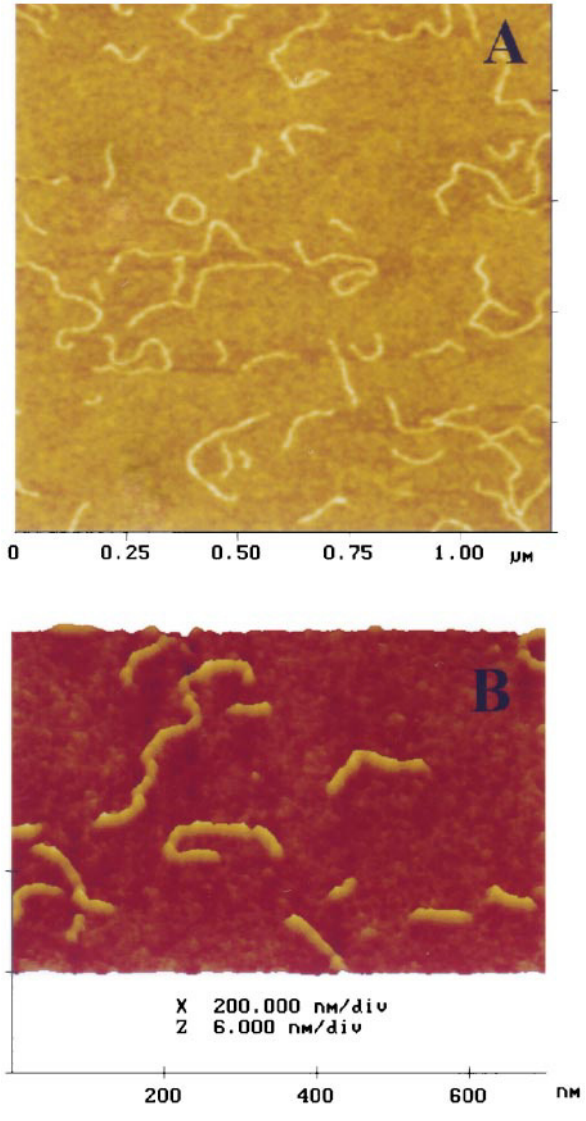

FIGURE 1 AFM images of DNA deposited onto mica. (*A*) Typical height mode image of plasmid fragments (scan size 1250 × 1250 × 5 nm). (*B*) Three-dimensional representation of the same sample (scan size 700 × 700 × 6 nm, pitch angle 45°).

nm, 184 ± 7 nm, 134 ± 6 nm, 73 ± 6 nm, and 50 ± 3 nm, consistent with the expected values for B-helix DNA fragments.

To verify that DNA deposition was carried out under equilibrium conditions, we used the statistical polymer chain analysis applied to DNA on the 1429-bp fragment, as described by Rivetti et al. (1996).

DNA molecules can freely equilibrate on the mica as in a 2D solution before they are captured, resulting in an ensemble of lowest energy conformations, or be trapped without having equilibrated on the surface. In the first case, the mean-square end-to-end distance $\langle R^2 \rangle$ should be close to that of an ideal polymer chain in two dimensions. This distance is given by the equation (Rivetti et al., 1996):

$$\langle R^2 \rangle_{2D} = 4PL(1 - 2P(1 - e^{-L/2P})/L) \quad (1)$$

where P is the persistence length of the polymer, and L the length of the fragment.

In the second case, the $\langle R^2 \rangle$ distance would be described as a polymer chain in three dimensions projected onto the surface, and then the equation becomes (Rivetti et al., 1996):

$$\langle R^2 \rangle_{proj} = (4/3)PL(1 - P(1 - e^{-L/P})/L) \quad (2)$$

Assuming a persistence length of 53 nm and a length of 485 nm for the 1429-bp fragment, we found $\langle R^2 \rangle_{2D}$ = 81,785 nm^2 and $\langle R^2 \rangle_{proj}$ = 30,545 nm^2. We measured the end-to-end distances of the 485-nm-long fragment for more than 100 images, and found a mean square $\langle R^2 \rangle$ distance of 88,500 nm^2, consistent with the 2D model. Fig. 2 shows a histogram of these end-to-end distances, expressed as a percent of the total length. This result indicates that the DNA molecules are able to reach thermodynamic equilibration on the surface before being trapped. When TR is also present in solution, the same value for $\langle R^2 \rangle$ distance for DNA complexed by the repressor is found.

Characterization of repressor bound to DNA

When the *trp* repressor is present in the deposition drop, this protein is clearly seen in AFM height images. The density of repressor increases with the concentration in the solution (Fig. 3). Fig. 4 shows two images of the TR/operator complex. The protein is located in the center of a 1429-bp fragment, the position of the *trp* EDCBA operator site, implying a site-specific complex. Image *B* is a classic height representation of this DNA fragment and *A* is a phase mode image. When the tip scans the protein, a high phase signal is detected. This dephasing shows different dynamic properties between DNA and the repressor. This information aided us in unambiguously identifying the *trp* repressor bound to the DNA on large-scale images, using simultaneous acquisition of height and phase signals.

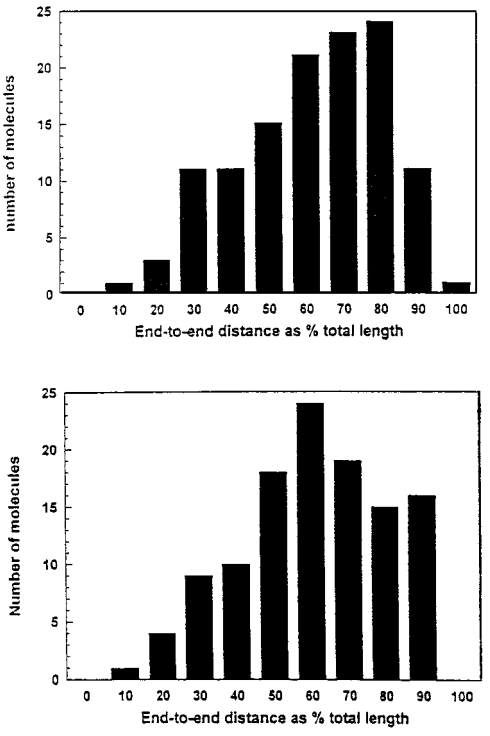

FIGURE 2 Repartition of the end-to-end distances as percent of the total lengths for the 1429-bp plasmid fragments carrying the *trp* EDCBA (*top*) and the *trp* R (*bottom*) operators.

Analysis of *trp* repressor binding states

Three different binding states can be reached by the repressor: it can be specifically or nonspecifically bound to the DNA, or free in solution. All of these states are apparent in Fig. 5. Four different specific TR/operator complexes located in the center of the 1429-bp fragment are shown by the blue arrows in images *A–D* (Fig. 5). These site-specific complexes are the most frequently seen at low protein concentrations (1 nM TR dimer). The red arrows in images *E* and *F* (Fig. 5) represent nonspecific TR/DNA complexes. In image *E*, one protein is bound on the 1429-bp fragment, but far away from the specific site at one-quarter the total length, and another one is bound on the end of the 540-bp fragment. Higher-order oligomers are sometimes seen when the repressor is bound to nonspecific sites (Fig. 5 *F*, red arrow). This is not the case when the repressor is located on its operator.

Repressor proteins free in solution and directly deposited onto the mica surface are shown by green arrows in Fig. 5, images *C–F*. In this case, assemblies of different sizes are often seen, which are characteristic of TR oligomers, as previously shown by fluorescence spectroscopy (Fernando and Royer, 1992).

Section analysis of DNA

To determine the size of the TR/operator complexes, apparent height and width measurements were performed both on

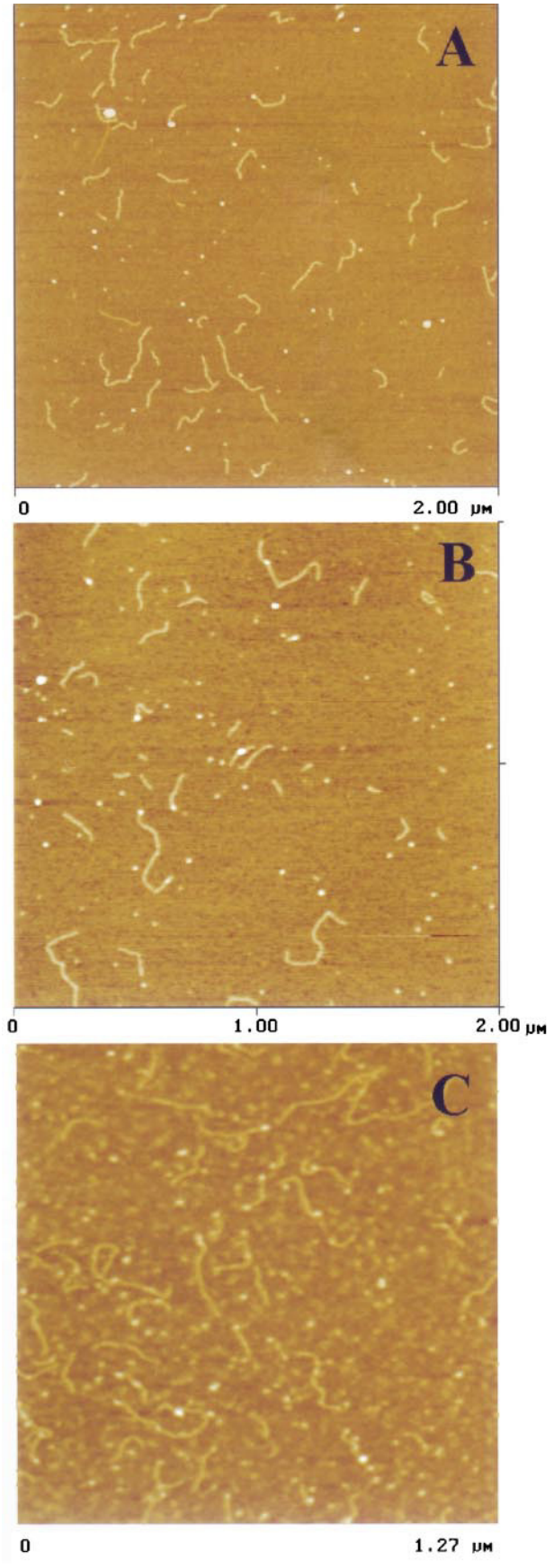

FIGURE 3 AFM images of 50 pM DNA and *trp* repressor at different concentrations. An increase of protein density deposited onto mica is clearly seen on these images. (*A*) TR 1 nM, scan size 2000 × 2000 × 3 nm; (*B*) TR 5 nM, scan size 2000 × 2000 × 3 nm; (*C*) TR 100 nM, scan size 1270 × 1270 × 5 nm.

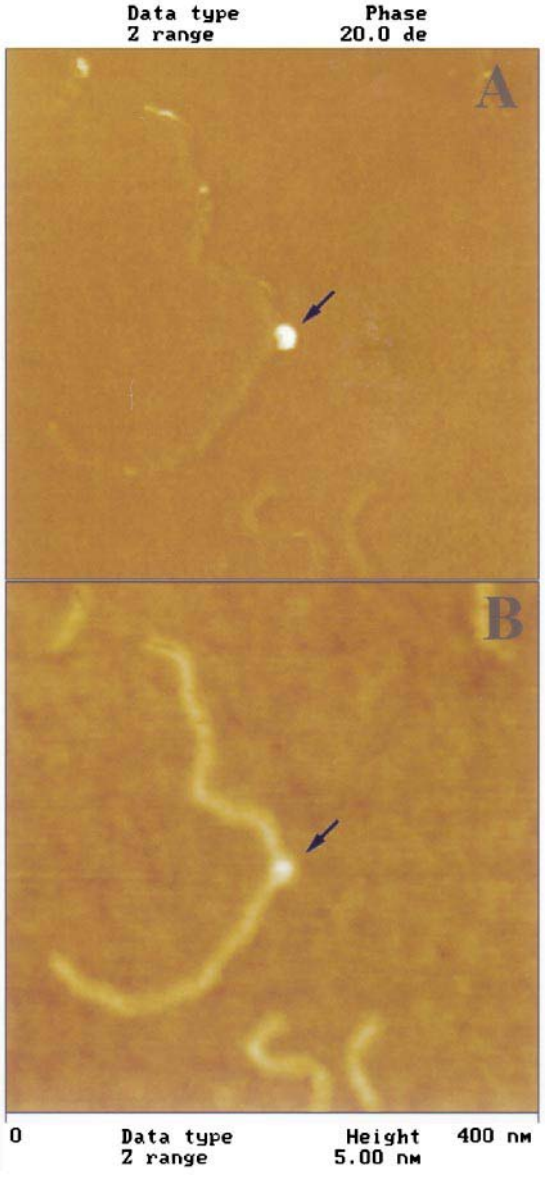

FIGURE 4 AFM images of a typical specific TR/DNA complex in height mode (*B*) and phase mode (*A*) (scan size 400 × 400 nm). The repressor protein bound in the middle of the 1429-bp fragment is clearly seen. The phase image shows the difference of dynamic properties between the DNA and the protein (see text).

DNA and protein, using the Nanoscope III section analysis software. We found a mean height of 0.6–0.8 nm and a mean width of 10–13 nm for DNA (Fig. 6, *A* and *B*). The theoretical height for a double-stranded DNA molecule is 2 nm. AFM images of soft biomolecules are usually seen wider and smaller than the sample itself (Delain et al., 1992; Vesenka et al., 1992; Mastrangelo et al., 1994; Wyman et al., 1995). A closer approximation of the actual height and

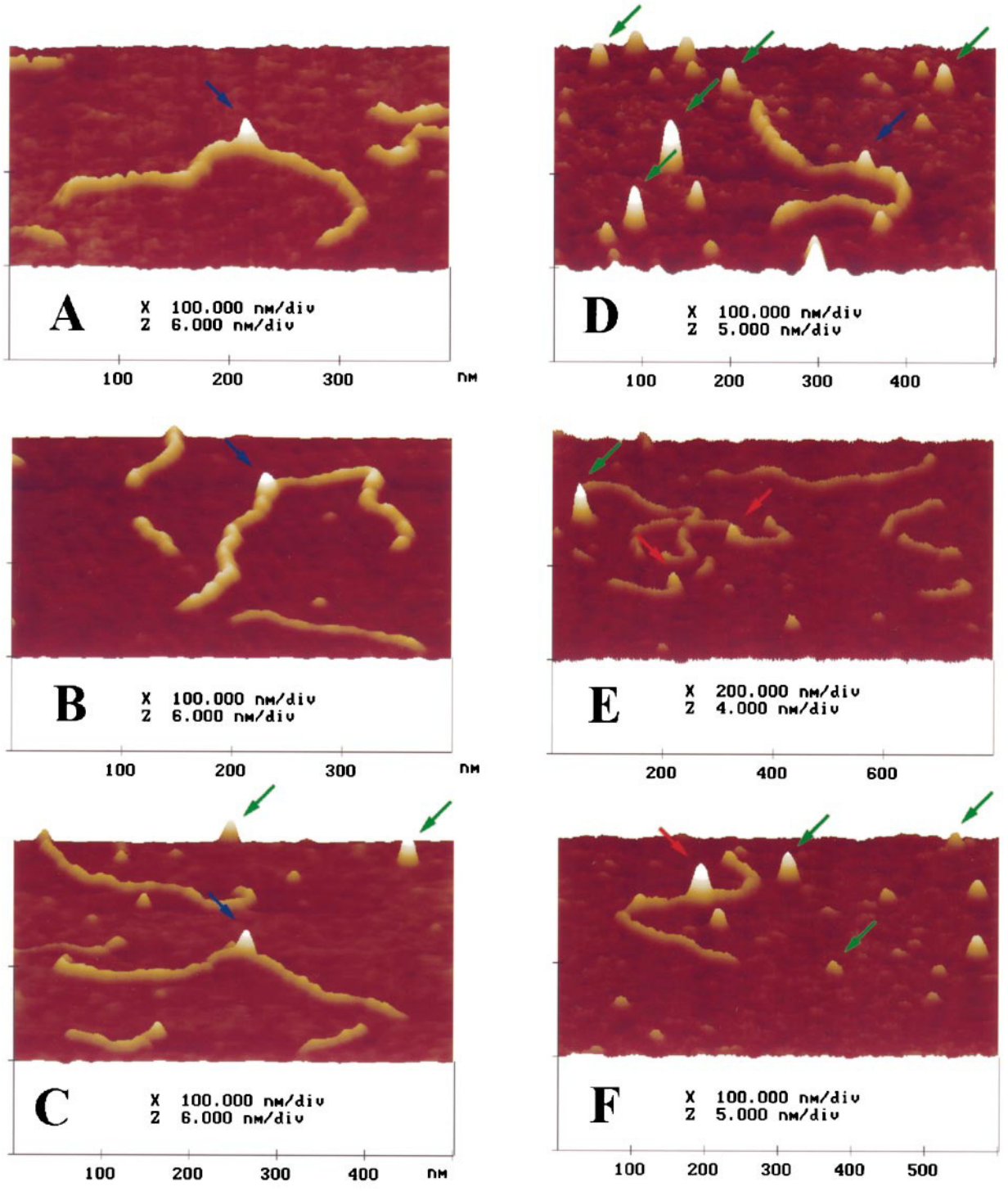

FIGURE 5 Three-dimensional representations (30° pitch) of AFM images of TR/operator complexes and TR oligomers. The shape of the protein is exaggerated due to the anisotropic scaling. The blue arrows show specific complexes, the red arrows represent nonspecific complexes, and the green arrows show free *trp* repressor oligomers of different sizes.

width of DNA molecules was achieved in a study using tapping mode under liquid and a modified substrate (Lyubchenko and Shlyakhtenko, 1997). However, the dimensions found in many other tapping mode studies, even under liquid, are close to those we observe here. To explain the smaller height and larger width typically found for DNA, many reasons can be put forward (Vesenka et al., 1992; Engel et al., 1997). During the scan, the tip involves a deformation of the molecules, and the resulting apparent height is usually smaller than the sample itself. Moreover, the DNA molecules are sometimes observed as "embedded" in a layer on the mica surface, which may be a result of the

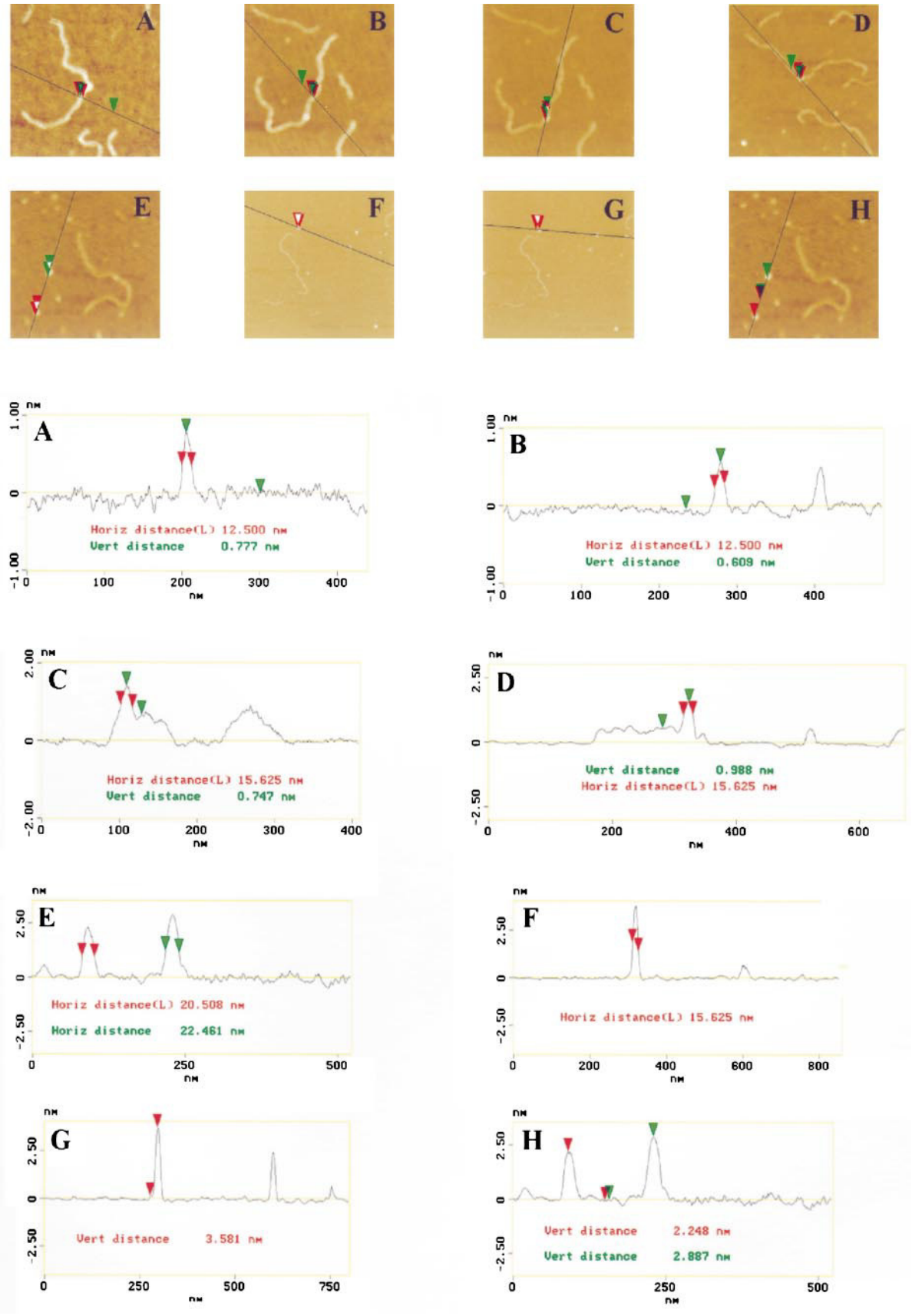

FIGURE 6 Section analysis on high-magnification AFM images of TR and DNA. (*A–D*) Height (green) and width at the half-maximum (red) of DNA (*A* and *B*) and specific protein/DNA complexes (*C* and *D*). (*E–H*) Width at the half-maximum (*E* and *F*) and height (*G* and *H*) of some free *trp* repressor oligomers.

presence of water and salts. This phenomenon may also contribute to the small apparent height of the DNA.

The presence of cationic salts in the deposition drop leads to a salt complexation with the DNA, which then appears wider than the 2 nm found with the crystallographic data. Moreover, the radius of curvature of the tip (usually >10 nm) exceeds the diameter of the DNA. This feature leads to a larger apparent width of the plasmids. The tip radius can be calculated using the simplified model described by Engel et al. (1997). For this purpose we assumed that DNA has a cylindrical shape and used Eq. 3, which links the apparent and the real widths of a spherical sample:

$$S = 2 \times (R \times D + D^2/4)^{1/2} \quad (3)$$

where R is the tip radius, D is the real size of the molecule studied, and S is the bandwidth at the half-maximum seen on the section. We measured a mean value of 11 nm for the DNA. Taking the known 2-nm diameter for B-form DNA, and using Eq. 3, we found a tip radius, $R = 14.6$ nm, consistent with the theoretical value for these tips.

Section analysis of *trp* repressor

Section analysis was used to determine the size of the repressor molecules, both free on the surface and specifically bound to their operators, for *trp* EDCBA and *trp* R plasmids. In this latter case, typical heights ranged from 0.6 to 1 nm above the DNA and widths from 16 to 19 nm; no significant difference was seen between proteins bound to *trp* EDCBA and *trp* R operators (Fig. 6, *C* and *D*). Assuming the 14.6 nm radius for the tip calculated from the preceding experiment, Eq. 3 was used to estimate the real width of the repressor. We calculate that the protein seen in the images is 5–6 nm long. The crystallographic data for the *trp* repressor bound to its operator show a 5-nm-long protein for the 1/1 complex and a 8–9-nm-long protein tetramer for the tandem complex. The apparent length of the repressor observed on the AFM images is consistent with the presence of up to two TR dimers, but not with higher-order oligomers.

When the repressor concentration increases in the deposition solution (1–5 nM dimer), many free TR repressor oligomers deposited on the mica surface are seen in the AFM images. Typical widths ranging from 15 to 25 nm were found (Fig. 6, *E* and *F*). The height of these assemblies was situated between 1 and 4 nm (Fig. 6, *G* and *H*). These values clearly show that *trp* repressor has a strong tendency to oligomerize when free in solution, consistent with previous studies (Fernando and Royer, 1992).

Study of TR binding without co-repressor

The same protocol was used for the deposition of DNA and *trp* repressor using an L-trp free buffer. Repressor concentrations ranging from 1 nM to 100 nM dimer were used. In every case, DNA spread out normally, but no protein was observed, either on the plasmids or free on the mica surface. The fact that the aporepressor is not bound to its operator in this concentration range is consistent with previous studies using fluorescent oligonucleotides ($K_d > 100$ nM) (Le Tilly and Royer, 1993). Zhang and co-workers have already shown that co-repressor binding results in a change in the tertiary conformation of the repressor, thus increasing the specific DNA binding affinity of holo TR compared to apo TR (Zhang et al., 1987).

The absence of free TR molecules on the mica surface is more surprising. Fluorescence studies on extrinsically labeled TR shows that it forms higher-order oligomers in solution both in the absence and in the presence of L-trp, but that the binding of co-repressor destabilizes these oligomers (Fernando and Royer, 1992). The tertiary conformational changes between holo and apo repressor, and the high oligomerization tendency of the aporepressor, may result in a large-scale aggregation which then precludes the interaction with the mica surface.

Specificity of TR for *trp* R and *trp* EDCBA operators

The natural sites for high-affinity *trp* repressor binding are located in the center of the 485-nm-long fragment. The binding of this protein was studied both on this position (specific binding), and anywhere else on the different DNA fragments (nonspecific binding). Two concentrations of TR (5 nM and 1 nM dimer) were used for each of the plasmids (*trp* EDCBA and *trp* R), and 350–550 DNA fragments of different lengths were studied in every case. The results are summarized in Table 1.

Two major findings arise from this study: first, there is no significant difference in apparent specificity of the TR for the two operators. With the two concentrations used, the percent of 485-nm plasmid fragments bound by the repressor at the specific site versus the total 485-nm fragments bound by at least one repressor is the same for the operators *trp* R and *trp* EDCBA (respectively 53% and 46% with TR 1 nM, and 28% and 27% with TR 5 nM). Second, there is a threefold increase in specificity of the *trp* repressor for both operators when the concentration of this protein decreases from 5nM to 1 nM (7% to 21% for *trp* R, and 5% to 14% for *trp* EDCBA). This result was expected because these concentrations are in the range of the K_d of TR specific binding to its operator (Le Tilly and Royer, 1993). However, the high number of *trp* repressor molecules bound to nonspecific DNA in this range of concentration is surprising. It may be because of a local concentration effect occurring upon deposition near the mica surface.

CONCLUSIONS

Atomic force microscopy has been shown to be a useful technique to study nucleoprotein complexes at molecular resolution. The use of this tool allowed us to visualize the formation of specific and nonspecific *trp* repressor/DNA

TABLE 1

Length (nm)*	Bound with TR (1 nM)#	Bound with TR (5 nM)#	Site-Specific Complexes (1 nM TR)	Site-Specific Complexes (5 nM TR)
		trp R operator		
485	32%	86%	53%§	28%§
185	11%	43%	—	—
140–145	6%	42%	—	—
80	1%	18%	—	—
55	2%	8%	—	—
Total	8%	37%	21%¶	7%¶
		trp EDCBA operator		
485	43%	92%	46%§	27%§
185	20%	77%	—	—
140–145	14%	57%	—	—
80	6%	36%	—	—
55	3%	22%	—	—
Total	15%	55%	14%¶	5%¶

*The length of the plasmid fragment was calculated as 0.34 nm × number of basepairs.

#Percent of plasmid fragments bound by at least one TR molecule.

§Percent of 485-nm plasmid fragments bound by the repressor at the specific site versus all the 485 nm plasmid fragments bound by at least one repressor molecule.

¶Percent of 485-nm plasmid fragments bound by the repressor at the specific site versus all the plasmid fragments bound by at least one repressor molecule.

complexes, as well as unbound oligomers of TR. The goal of this study was to investigate the protein/protein interactions implicated in this mechanism of regulation, both when TR is bound to the DNA, and when free in solution.

Most studies using biochemical or spectroscopic techniques have suggested a role for these protein/protein interactions in both specific and nonspecific TR/DNA complex formation (Kumamoto et al., 1987; Staake et al., 1990; Haran et al., 1992; Le Tilly and Royer, 1993; Liu and Matthews, 1993; Czernik et al., 1994; Yang et al., 1996; Bareket-Samish et al., 1997; Reedstrom et al., 1997; Haran, 1998). We used AFM to investigate the size of the specific TR/operator complexes, which is of major importance in understanding this mechanism of regulation. Although the resolution of our AFM apparatus is somewhat limited for this system, we were able to conclude that the stoichiometry of the specific complexes did not exceed two dimers, while that of nonspecific complexes and unbound TR was quite variable and includes extremely large assemblies. AFM has been used previously to determine the stoichiometry of protein/DNA assemblies. In these cases, the proteins studied were wider than the *trp* repressor (Wyman et al., 1995, 1997; Rippe et al., 1997), or the binding sites were more clearly separated than in the case of the *trp* operator sequence (Erie et al., 1994), allowing unambiguous characterization of the protein oligomerization states in the AFM images, with a resolution similar to the one we achieved in the present study. The evolution of the AFM technique, leading to an improvement in the resolution, will probably allow the use of this technique in the near future to investigate the stoichiometry of DNA-binding proteins as small as the *trp* repressor.

The observation of large TR assemblies of varying sizes, both alone on the mica surface and bound to nonspecific sites on the DNA, is in contrast to the reproducible small complexes of TR bound at its specific operator sites. Such behavior supports a model based on solution biophysical measurements previously proposed by our group in which multiple modes of interaction between repressor dimers play a role in modulating the level of repression (Fernando and Royer, 1992; Le Tilly and Royer, 1993; Martin et al., 1994; Reedstrom and Royer, 1995; Reedstrom et al., 1996). All these findings underline the role of these protein/protein interactions as an additional competing mechanism for transcriptional regulation.

The authors thank Barry Hurlburt (Department of Biochemistry and Molecular Biology, University of Arkansas-Medical Sciences) for providing the plasmids containing the operator sites, Etienne Delain, Alain Fourcade, and Eric Le Cam (Institut Gustave Roussy, France) for technical assistance in DNA deposition, and the members of the Royer group (University of Wisconsin-Madison) for repressor production and purification.

This work was supported by grants from La Fondation pour la Recherche Medicale, l'Association pour la Recherche sur le Cancer, and la Région Languedoc-Roussillon.

REFERENCES

Bareket-Samish, A., I. Cohen, and T. E. Haran. 1997. Repressor assembly at *trp* binding sites is dependent on the identity of the intervening dinucleotide between the binding half sites. *J. Mol. Biol.* 267:103–117.

Bennett, G. N., and C. Yanofsky. 1978. Sequence analysis of operator constitutive mutants of the tryptophan operon of *Escherichia Coli. J. Mol. Biol.* 121:179–192.

Bustamante, C., C. Rivetti, and D. J. Keller. 1997. Scanning force microscopy under aqueous solutions. *Curr. Opin. Struct. Biol.* 7:709–716.

Cherny, D. I., A. Fourcade, F. Svinarchuk, P. E. Nielsen, C. Malvy, and E. Delain. 1998. Analysis of various sequence-specific triplexes by electron and atomic force microscopies. *Biophys. J.* 74:1015–1023.

Czernik, P. J., D. S. Shin, and B. K. Hurlburt. 1994. Functional selection and characterization of DNA binding sites for *trp* repressor of *Escherichia coli. J. Biol. Chem.* 269:27869–27875.

Delain, E., A. Fourcade, J.-C. Poulin, A. Barbin, D. Coulaud, E. Le Cam, and E. Paris. 1992. Comparative observations of biological specimens, especially DNA and filamentous actin molecules in atomic force, tunnelling and electron microscopy. *Microsc. Microanal. Microstruct.* 3:457–470.

Engel, A., C.-A. Schoenenberger, and D. J. Müller. 1997. High resolution imaging of native biological samples surfaces using scanning probe microscopy. *Curr. Opin. Struct. Biol.* 7:279–284.

Erie, D. A., G. Yang, H. C. Schultz, and C. Bustamante. 1994. DNA bending by Cro protein in specific and non-specific complexes: implications for protein site recognition and specificity. *Science.* 266: 1562–1566.

Fernando, T., and C. A. Royer. 1992. Role of protein-protein interactions in the regulation of transcription by *trp* repressor investigated by fluorescence spectroscopy. *Biochemistry.* 31:3429–3441.

Fritzsche, W., A. Schaper, and T. M. Jovin. 1994. Probing chromatin with the scanning force microscope. *Chromosoma.* 103:231–236.

Fritzsche, W., L. Takac, and E. Henderson. 1997. Application of atomic force microscopy to visualization of DNA, chromatin, and chromosomes. *Crit. Rev. Eukaryotic Gene Expression.* 7:231–240.

Gunsalus, R. P., and C. Yanofsky. 1980. Nucleotide sequence and expression of *Escherichia coli trpR*, the structural gene for the *trp* aporepressor. *Proc. Natl. Acad. Sci. USA.* 77:7117–7121.

Guthold, M., M. Bezanilla, D. A. Erie, B. Jenkins, H. G. Hansma, and C. Bustamante. 1994. Following the assembly of RNA polymerase-DNA complexes in aqueous solutions with the scanning force microscope. *Proc. Natl. Acad. Sci. USA.* 91:12927–12931.

Hansma, H. G., and J. H. Hoh. 1994. Biomolecular imaging with the atomic force microscope. *Annu. Rev. Biophys. Biomol. Struct.* 23: 115–139.

Hansma, H. G., K. J. Kim, D. E. Laney, R. A. Garcia, M. Argaman, M. J. Allen, and S. M. Parsons. 1997. Properties of biomolecules measured from atomic force microscope images: a review. *J. Struct. Biol.* 119: 99–108.

Hansma, H. G., D. E. Laney, M. Bezanilla, R. L. Sinsheimer, and P. K. Hansma. 1995. Applications for atomic force microscopy of DNA. *Biophys. J.* 68:1672–1677.

Haran, T. E. 1998. Statistical and structural analysis of *trp* binding sites: comparison of natural and in vitro selected sequences. *J. Biomol. Struct. Dyn.* 15:689–701.

Haran, T. E., A. Joachimiak, and P. B. Sigler. 1992. The DNA target of the *trp* repressor. *EMBO J.* 11:3021–3030.

Heatwole, V. M., and R. L. Sommerville. 1991. Cloning, nucleotide sequence, and characterization of *mtr*, the structural gene for a tryptophan-specific permease of *Escherichia coli*. K-12. *J. Bacteriol.* 173: 108–115.

Joachimiak, A., R. L. Kelley, R. P. Gunsalus, C. Yanofsky, and P. B. Sigler. 1983. Purification and characterization of *trp* aporepressor. *Proc. Natl. Acad. Sci. USA.* 80:668–672.

Kasas, S., N. H. Thomson, B. L. Smith, H. G. Hansma, X. Zhu, M. Guthold, C. Bustamante, E. K. Kool, M. Kashlev, and P. K. Hansma. 1997. *Escherichia coli* RNA polymerase activity observed using atomic force microscopy. *Biochemistry.* 36:461–468.

Kumamoto, A., W. Miller, and R. P. Gunsalus. 1987. *E. coli* tryptophan repressor binds multiple sites within the *aro*H and *trp* operators. *Genes Dev.* 1:556–564.

Lawson, C. L., and J. Carey. 1993. Tandem binding in crystals of a *trp* repressor/operator half-site complex. *Nature (Lond.).* 366:178–182.

Le Cam, E., D. Frechon, M. Barray, A. Fourcade, and E. Delain. 1994. Observation of binding and polymerization of Fur repressor onto operator-containing DNA with electron and atomic force microscopes. *Proc. Natl. Acad. Sci. USA.* 91:11816–11820.

Le Tilly, V., and C. A. Royer. 1993. Fluorescence anisotropy assays implicate protein-protein interactions in regulating *trp* repressor DNA binding. *Biochemistry.* 32:7753–7758.

Liu, Y.-C., and K. S. Matthews. 1993. Dependence of *trp* repressor-operator affinity, stoichiometry, and apparent cooperativity on DNA sequence and size. *J. Biol. Chem.* 268:23239–23249.

Lyubchenko, Y. L., B. L. Jacobs, S. M. Lindsay, and A. Stasiak. 1995. Atomic force microscopy of nucleoprotein complexes. *Scanning Microsc.* 9:705–727.

Lyubchenko, Y. L., and L. S. Shlyakhtenko. 1997. Visualization of supercoiled DNA with atomic force microscopy in situ. *Proc. Natl. Acad. Sci. USA.* 94:496–501.

Lyubchenko, Y. L., L. S. Shlyakhtenko, T. Aki, and S. Adhya. 1997. Atomic force microscopic demonstration of DNA looping br GalR and HU. *Nucleic Acids Res.* 25:873–876.

Martin, K. S., C. A. Royer, K. P. Howard, J. Carey, T.-C. Liu, K. Matthews, E. Heyduk, and J. C. Lee. 1994. Electrostatic forces contribute to interactions between trp repressor dimers. *Biophys. J.* 66: 1167–1173.

Mastrangelo, I. A., M. Bezanilla, P. K. Hansma, P. V. C. Hough, and H. G. Hansma. 1994. Structures of large T antigen at the origin of SV40 DNA replication by atomic force microscopy. *Biophys. J.* 68:293–298.

Mou, J., D. M. Czajkowsky, Y. Zhang, and Z. Shao. 1995. High-resolution atomic-force microscopy of DNA: the pitch of the double helix. *FEBS Lett.* 371:279–282.

Palecek, E., D. Vlk, V. Stankova, V. Brazda, B. Vojtesek, T. R. Hupp, A. Schaper, and T. M. Jovin. 1997. Tumor suppressor protein p53 binds preferentially to supercoiled DNA. *Oncogene.* 15:2201–2209.

Paluh, J. H., and C. Yanofsky. 1986. High-level production and rapid purification of the *Escherichia coli trp* repressor. *Nucleic Acids Res.* 14:7851–7860.

Reedstrom, R. J., M. P. Brown, A. Grillo, D. Roen, and C. A. Royer. 1997. Affinity and specificity of *trp* repressor-DNA interactions studied with fluorescent oligonucleotides. *J. Mol. Biol.* 273:572–585.

Reedstrom, R. J., K. S. Martin, S. Vangala, S. Mahoney, E. W. Wilker, and C. A. Royer. 1996. Characterization of charge change super-repressor mutants of *trp* repressor: effects on oligomerization, conformation, ligation and stability. *J. Mol. Biol.* 264:32–45.

Reedstrom, R. J., and C. A. Royer. 1995. Evidence for coupling of folding and function in *trp* repressor: physical characterization of the superrepressor mutant AV77. *J. Mol. Biol.* 253:741–750.

Rippe, K., M. Guthold, P. H. von Hippel, and C. Bustamante. 1997. Transcriptional activation *via* DNA-looping: visualization of intermediates in the activation pathway of *E. coli* RNA polymerase · σ^{54} holoenzyme by scanning force microscopy. *J. Mol. Biol.* 270:125–138.

Rivetti, C., M. Guthold, and C. Bustamante. 1996. Scanning force microscopy of DNA deposited onto mica: equilibrium versus kinetic trapping studied by statistical polymer chain analysis. *J. Mol. Biol.* 264:919–932.

Rose, J. K., and C. Yanofsky. 1974. Interaction of the operator of the tryptophan operon with repressor. *Proc. Natl. Acad. Sci. USA.* 71: 3134–3138.

Schaper, A., J. P. P. Starink, and T. M. Jovin. 1994. The scanning force microscopy of DNA in air and in n-propanol using new spreading agents. *FEBS Lett.* 355:91–95.

Staake, D., B. Walter, B. Kisters-Woike, B. V. Wilcken-Bergman, and B. Müller-Hill. 1990. How *trp* repressor binds to its operator. *EMBO J.* 9:1963–1967.

Tamayo, J., and R. Garcia. 1997. Effects of elastic and inelastic interactions on phase contrast images in tapping-mode scanning force microscopy. *Appl. Phys. Lett.* 16:2394–2396.

Vesenka, J., M. Guthold, C. L. Tang, D. Keller, E. Delain, and C. Bustamante. 1992. Substrate preparation for reliable imaging of DNA molecules with the scanning force microscope. *Ultramicroscopy* 42: 1243–1249.

Wyman, C., E. Grotkopp, C. Bustamante, and H. C. M. Nelson. 1995. Determination of heat-shock transcription factor 2 stoichiometry at looped DNA complexes using scanning force microscopy. *EMBO J.* 14:117–123.

Wyman, C., I. Rombel, A. K. North, C. Bustamante, and S. Kustu. 1997. Unusual oligomerization required for activity of NtrC, a bacterial enhancer-binding protein. *Science.* 275:1658–1661.

Yang, J., A. Gunasekera, T. A. Lavoie, L. Jin, D. E. A. Lewis, and J. Carey. 1996. In vivo and in vitro studies of TrpR-DNA interactions. *J. Mol. Biol.* 258:37–52.

Yang, J., and Z. Shao. 1995. Recent advances in biological atomic force microscopy. *Micron.* 26:35–49.

Yang, J., K. Takeyasu, and Z. Shao. 1992. Atomic force microscopy of DNA molecules. *FEBS Lett.* 301:173–176.

Zhang, R. G., A. Joachimiak, C. L. Lawson, R. W. Schewitz, Z. Otwinowski, and P. B. Sigler. 1987. The crystal structure of *trp* aporepressor at 1.8 Å shows how binding tryptophan enhances DNA affinity. *Nature (Lond.).* 327:591–597.

Zurawski, G., R. P. Gunsalus, K. D. Brown, and C. Yanofsky. 1981. Structure and regulation of *aro*H, the structural gene for the tryptophan-repressible 3-deoxy-D-arabino-heptulosonic acid-7-phosphate synthetase of *Escherichia coli. J. Mol. Biol.* 145:47–73.